Proton Direct Ionization in Sub-Micron Technologies: Numerical Method for RPP Parameter Extraction

Sascha Lüdeke, *Member, IEEE,* and Arto Javanainen, *Member, IEEE*

***Abstract*—This work introduces a numerical method to iteratively extract parameters of a rectangular parallelepiped (RPP) sensitive volume (SV) from experimental proton direct ionization SEU data. The method combines two separate numerical models. The first model estimates the average LET values for energetic ions, including protons and also heavy ions, in elemental solid targets. The second model describes the statistical variance in the energy deposition events of projectile-induced primary ionization within a RPP shaped target volume. To benchmark the method, simulated cross-section values based on RPP parameters derived with this method are compared with literature data from four SRAM devices. The RPP geometries determined by this method reproduced the experimental cross-section values in the literature with good accuracy, therefore showing that this method can be used to reliably and quickly determine the RPP parameters for SVs in memories sensitive to proton direct ionization (PDI). The method is currently strictly limited to direct ionization effects, i.e. not taking into account any nuclear reaction mechanisms, and elemental materials due to the underlying models' definitions.**

***Index Terms*—proton direct ionization (PDI), single event upset (SEU), linear energy transfer (LET), straggling, Monte Carlo (MC) method, rectangular parallelepiped (RPP)**

I. Introduction

The impact of proton direct ionization (PDI) on the single event upset (SEU) cross sections of highly-scaled sub-micron technology has been demonstrated in [1]–[12], among others. Therefore, it is of great importance to consider the contribution of low energy protons (LEP) ($E_{p^+} < 3MeV$) to the on-orbit soft error rate (SER) [1]–[7], [13]. Also the impact of LEP PDI effects on the SER in avionics have been shown [14].

One of the main methods to investigate the SERs is to use the rectangular parallelepiped (RPP) method [4], [5], [9], [15], [16]. This approach assumes a RPP-shaped sensitive volume (SV) and uses it as a surrogate for the device under testing (DUT) in Monte Carlo (MC) simulations of the radiation environment. This method does not rely on any knowledge of the inner composition and design of the DUT and can therefore be used when this information is not available or insufficient. The RPP geometry does not represent the actual charge collection area of the device, it emulates the devices SEU response in radiation transport simulations. Therefore, the parameters of the RPP do not have any physical meaning in regards to the actual structure of the device, but the RPP geometry can be used to calculate SER under various radiation environments due to its similar SEU response as the DUT.

The parameters for the single SV RPP approach used in this work are lateral length and width (a_{SV}) of the SV, height (h_{SV}) of the SV, critical charge threshold (Q_{crit}) of the SV required to trigger an upset and the thickness (h_{OL}) of any material or overlayers between the incident beam and the SV of the DUT. A schematic representation of the RPP geometry is given in Fig. 1.

While direct approaches to deduce the parameters for the RPP geometry from heavy-ion and proton cross section data, e.g. [17]–[19], have been formulated, an approach to estimate these directly from low energy proton data has not been found. Therefore, the common procedure to determine RPP parameters consists of an iterative (usually manual) process of adjusting the parameters of the RPP geometry and simulating the resulting cross sections of the geometry using the MC method until the simulated and experimental cross sections agree. This process depends on user experience, hence the obtained parameters are not necessarily unequivocal, depending on the users assessment of a good visual fit between the simulated and experimental data. Furthermore, due to the relative complexity and computational demands of MC simulations, this procedure can be difficult and time consuming.

In this work, a less time intensive and numerical approach to iteratively determine appropriate RPP parameters from PDI cross-section data is proposed. Instead of using the MC method to calculate the energy depositions in the SV of the RPP geometry and consecutively the cross sections, the presented method combines two numerical models to achieve this.

The first, a linear energy transfer (LET) model is based on a semi-empirical modification of Bloch's stopping number after [20]. In this work the terms LET, stopping force and stopping power are used as synonyms is used to estimate the average energy deposition of ions traversing target materials.

The second model is formulated after [21], and it describes the standard deviation of an ion's energy deposition in a target volume of a given thickness.

The method then provides an estimate of the energy deposition distributions within the SV based on a RPP geometry for protons with different initial energies. The PDI SEU cross sections of the device represented by the RPP

This project has received funding from the European Union's Horizon 2020 research and innovation programme under the Marie Sklodowska-Curie grant agreement number 721624.

The simulations were performed at the HPC Cluster CARL, located at the University of Oldenburg (Germany) and funded by the DFG through its Major Research Instrumentation Programme (INST 184/157-1 FUGG) and the Ministry of Science and Culture (MWK) of the Lower Saxony State.

S. Lüdeke is with the University of Jyväskylä, Accelerator Laboratory, Department of Physics, P.O. Box 35, FI-40014 University of Jyväskylä, Finland, e-mail: sascha.a.f.ludeke@jyu.fi.

A. Javanainen is with the University of Jyväskylä, Accelerator Laboratory, Department of Physics, P.O. Box 35, FI-40014 University of Jyväskylä, Finland and Electrical and Computer Engineering Department, Vanderbilt University, Nashville, TN 37235 USA, e-mail: arto.javanainen@jyu.fi

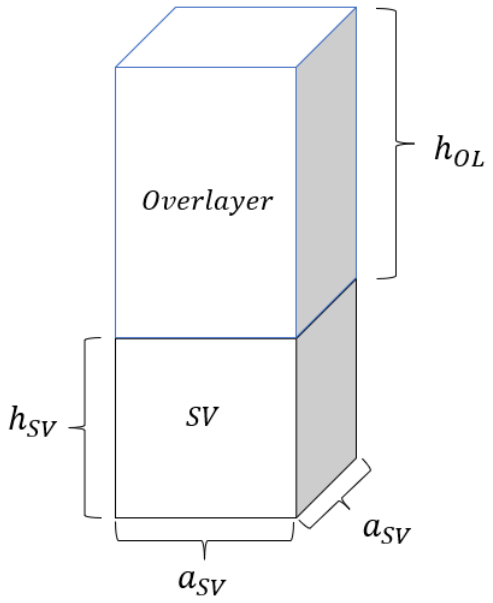

Fig. 1. Schematic representation of the RPP geometries assumed in this work (not to scale).

geometry can be then estimated from these distributions by applying the Q_{crit} of the RPP geometry to the energy deposition distribution. Applying this method for protons with different initial energies the PDI cross-section as a function of initial proton energy can be derived. With that, the parameters of the RPP geometry can then be adjusted and a new set of cross-section calculated. The parameters are adjusted until the estimated cross-section values agree with the experimental PDI cross-section data.

Due to the numerical and simpler nature of the proposed method, the parameters of the RPP geometry can be adjusted and the resulting cross-section calculated without the use of the MC method, making the process less time consuming. Further, the proposed method can be implemented in any programming language with numeric abilities and requires less computation power than MC simulations.

This method is not meant to replace the MC method in general, but rather to substitute it during this iterative adjustment process of the RPP parameters to find the most fitting RPP geometry for a given data set.

In this work experimental and simulated proton SEU data [4], [5], [9] for several SRAMs were used to benchmark the method's ability to determine RPP geometries from PDI cross-section data. The determined RPP parameters for the data sets by this method were verified via MC simulations and the results compared against the simulations presented in the literature. All MC simulations in this work were performed with the Geant4 toolkit [22]. Additionally, the new LET model for protons and heavy ions in elemental targets is presented and verified against experimental LET data [23].

II. LET Model

In the following section the semi-empirical LET model for protons and heavy ions in elemental targets is introduced. The model is used in the methodology presented here to estimate the energy lost to the overlayers by the proton as well as the average energy deposited within the SV by the proton.

A. Model and Calculations

The general description of the linear energy transfer $\left(\frac{dE}{dx}\right)$ in units of $\mathrm{MeVcm^2/mg}$ can be expressed as:

$$\frac{dE}{dx} = 3.0705 \cdot 10^{-4} \cdot \frac{Z_1 \cdot Z_2}{A_2 \beta^2} \cdot L, \tag{1}$$

where Z_1 and Z_2 are the atomic numbers for the projectile and target, respectively, A_2 the mass number of the target and β the velocity of the projectile relative to the speed of light [24]. The parameter L is referred to as the *stopping number*.

Essentially, the stopping number governs the overall dependence of the LET on projectile velocity, atomic number and the target properties. Depending on the theory (or model), in general the stopping number is usually given in form

$$L_i = \ln(\xi_i) \tag{2}$$

where ξ_i is the *stopping variable* for the theory in question. The theory proposed by Bohr [25] defines the stopping number as

$$L_{Bohr} = \ln(\xi_{Bohr}) = \ln\left(C\frac{m_e c^2 \beta^3}{Z_1 I \alpha}\right), \tag{3}$$

where $I = Z_2 \cdot 10\ eV$ represents the mean ionization energy of the target atoms, $C = 2e^{-\gamma}$ with $\gamma = 0.5772$, unitless, as the Euler-Mascheroni constant, $m_e = 511\ keV/c^2$ the electron mass, c the speed of light in $\mathrm{m/s}$ and $\alpha \approx 1/137$ the unitless fine-structure constant. Bohr's stopping number is valid for intermediate and high projectile energies.

The second theory, describing the high energy stopping number is the Bethe's formula that mostly covers very high energies. In case of Bethe's theory the stopping number reads as:

$$L_{Bethe} = ln(\xi_{Bethe}) = \ln\left(\frac{2m_e c^2 \beta^2}{I}\right). \tag{4}$$

Bohr's stopping theory was then combined by Bloch with Bethe's theory, which led to a new definition of the stopping number after Bloch's theory approximated by de Ferrariis and Arista [24]:

$$L_{Bloch} = \ln\left(C\frac{m_e c^2 \beta^3}{Z_1 I \alpha}\frac{1}{\sqrt{1+\left(\frac{C\beta}{2Z_1\alpha}\right)^2}}\right) \tag{5}$$

This stopping number now covers both the energy range of Bohr's and Bethe's theory, because for very high energies the Bloch's stopping variable will convert towards Bethe's stopping variable.

For the low energy stopping the most prominent theories are the ones by Lindhard and Scharff [26] (LSS) and Firsov [27]. Both theories show that for low energies the stopping power is proportional to Bohr's stopping variable. Therefore, in comparison with Eq. 1, the following applies:

$$\begin{aligned} L_{LSS} &\propto \xi_{Bohr} \\ L_{Firsov} &\propto \xi_{Bohr} \end{aligned} \tag{6}$$

This work proposes a modification to the approximation of Bloch's stopping number after [20] using two semi-empirical unitless parameters p_0 and p_1, with no direct physical meaning, in the following manner:

$$\ln(\xi_{Bloch}) \rightarrow p_0 \cdot \ln(1 + p_1 \xi_{Bloch}) \tag{7}$$

This modification results in the following expression for the modified Bloch's stopping number:

$$L = p_0 \cdot \ln\left(1 + p_1 C \frac{m_e c^2 \beta^3}{Z_1 I \alpha} \frac{1}{\sqrt{1 + \left(\frac{C\beta}{2 Z_1 \alpha}\right)^2}}\right) \tag{8}$$

This alteration impacts the convergence behavior of the stopping number in the low and high energy regime according to Eq. 9. In the low energy regime it allows the modified Bloch's stopping number to converge towards a form similar to the stopping numbers after LSS [26] and Firsov [27], both are considered to accurately describe the stopping of particles in the low energy regime [24]. The similarity is that both theories and the modified stopping number can be described as proportional to Bohr's stopping variable in the low energy range.

$$p_o \ln(1 + p_1 \cdot \xi_{Bloch}) \approx \begin{cases} p_0 p_1 \cdot \xi_{Bohr}, & v \rightarrow 0 \\ p_0 \ln(p_1 \cdot \xi_{Bethe}), & v \rightarrow \infty \end{cases} \tag{9}$$

Additionally, the modified stopping number behaves similar to Bloch's stopping number, after [20], in the intermediate energy range, which describes the stopping of particles in the intermediate and high energy regimes [24]. Finally, in the high energy range the modified stopping number converges towards an expression proportional to Bethe's stopping theory. Overall, the modification of Bloch's stopping number does not impact it's behavior in the intermediate energy range strongly, but allows one description of the stopping number to cover the entire energy range. Therefore, the semi-empirical modification of the stopping number can be used to describe all regimes of stopping with a single expression, unlike the theoretical descriptions that only cover partial energy regimes [24].

The stopping numbers L from different models and theories for H projectiles in a Si target as a function of the projectile energy are given in Fig. 2. The figure shows how the modified stopping number aligns with the theoretical stopping numbers in their respective energy interval.

In conclusion, this modification combines two stopping number expressions after [26], [27] and [20] describing low, intermediate and high energy stopping simultaneously.

The parameters p_0 and p_1 were determined for selected data sets from the Nuclear Data Services (NDS) Database [23]. One hundred and eight projectile-target combinations were selected, based on the amount and range of the available experimental data. For each combination Eq.(8) was fitted to the experimental data to determine p_0 and p_1. For projectile-target combinations not covered in this step, the values can be determined via linear interpolation of p_0 and p_1 over Z_1 and Z_2. The p_0 and p_1 parameters for all fitted data sets have been published at [28].

The LET values calculated from this model were compared to the experimental data from the NDS database [23] as well as LET values produced by the SRIM2013 [29] and DPASS [30]. The average difference ($\langle\Delta\rangle$) of the values from the model ($\frac{dE}{dx}_{mod}$) in comparison to the experimental values ($\frac{dE}{dx}_{exp}$) over the number of data points (N_{data}) in a certain

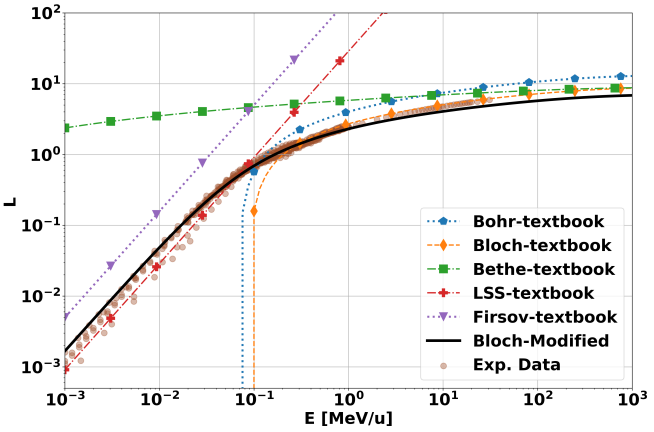

Fig. 2. Stopping number L as a function of proton energy E calculated from various theoretical approaches (Firsov, LSS, Bohr, Bethe and Bloch) in Si. Additionally, the modified stopping number presented in this work is shown. Finally, the stopping numbers of the experimental data from the NDS was calculated and displayed.

energy range was calculated using the following equation adapted from [31]:

$$\langle\Delta\rangle = \frac{1}{N_{data}} \sum_{N_{data}} \frac{\frac{dE}{dx}_{exp} - \frac{dE}{dx}_{mod}}{\frac{dE}{dx}_{exp}} \tag{10}$$

Furthermore, the standard deviation (s_Δ) of the difference between the modelled values and the experimental data is calculated after:

$$s_\Delta = \sqrt{\frac{1}{N_{data}} \sum_{N_{data}} \left(\frac{\frac{dE}{dx}_{exp} - \frac{dE}{dx}_{mod}}{\frac{dE}{dx}_{exp}} - \langle\Delta\rangle\right)^2} \tag{11}$$

These metrics were used to evaluate the ability of the model to estimate LET values at different projectile energies.

B. Results

Figure 3 presents the experimental LET values as a function of the projectile's energy for H projectiles in a Si target. Values calculated from the proposed LET model, DPASS [30] and SRIM2013 [29] softwares are presented as well. Overall, all models show good agreement with the experimental data and the established softwares. For H projectiles in Si targets the value for p_0 is 0.774 and 1.231 for p_1. The p_0 and p_1 parameters for the remaining data sets are published at [28]. Furthermore an example of the heavy ion LET values is given for O projectiles in an Al target is given in Fig. 4.

A comparison of values produced by different models over a wider variety of projectile-target combinations (H, He, O, Ar, Kr, Xe projectiles in C, Al, Ni, Si targets) against the experimental values was conducted using Eq. (10) and Eq. (11). The results are presented in Table I. The results are split into four energy regimes: $< 0.1\,\mathrm{MeV}$ (Low), $0.1\,\mathrm{MeV}$ to $10.0\,\mathrm{MeV}$ (Intermediate), $> 10.0\,\mathrm{MeV}$ (High) and covering all energies (Full). In the current iteration of the model projectiles ranging from H to Au and targets from Li until Au are covered. This describes the average performance of the model for common projectile and target combination in comparison to established models and software. A more detailed overview over the performance of the model in

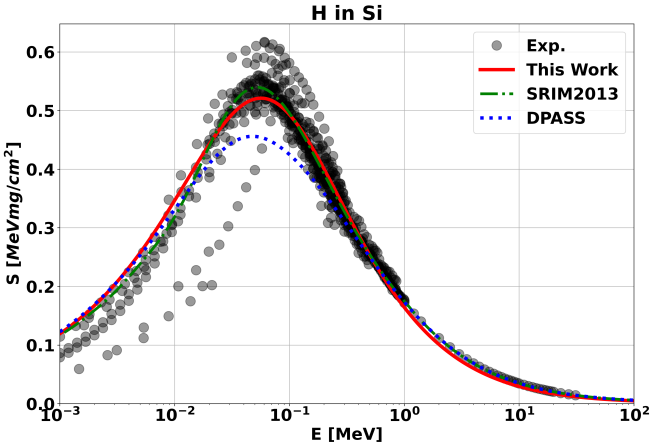

Fig. 3. LET values dE/dx in MeV/mg/cm^2 for H projectiles in Si targets over the projectile's kinetic energy E in MeV/u. Experimental data taken from the NDS database [23]. Modeled values from this work, SRIM [29] and DPASS [30] are shown.

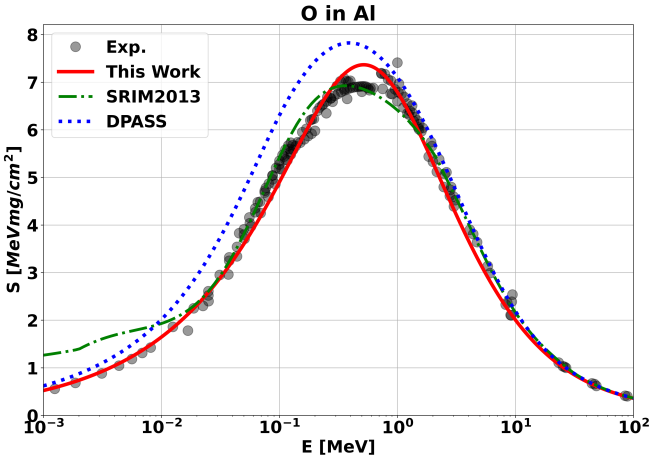

Fig. 4. SLET values dE/dx in MeV/mg/cm^2 for O projectiles in Al targets over the projectile's kinetic energy E in MeV/u. Experimental data taken from the NDS database [23]. Modeled values from this work, SRIM [29] and DPASS [30] are shown.

regards to every individual experimental value used in the fitting procedure has been published at [28].

Overall, the proposed model overestimates the experimental values in the low energy range and underestimate the data in the intermediate and high energy ranges. The proposed model performs comparable to SRIM and slightly better than DPASS in the considered projectile-target combinations. While Fig. 3 shows that the model accurately describes the LET values for protons in Si, which is of importance for the method proposed in this work, Table I, Fig. 4 as well as the data published at [28] further show that the LET model on its own can be successfully applied to a wider variety of projectile-target combinations, including heavy ion projectiles.

III. Straggling Model

In the following a model to estimate the standard deviation of the energy depositions in the SV adapted from [21] is presented. If only the average deposited energy in the SV is considered, the incoming protons of a specific energy are either able to cause an upset in the SV or not. This would result in a rectangular cross-section curve, which is not what can be seen in the experimental data reported in the literature. Straggling has been identified to be the a factor for the shape of the PDI cross-section response observed in the experimental data, which is considered in this method by considering the standard deviation of the energy depositions of the protons in the SV due to straggling.

A. Model and Calculations

An approximation of the relative standard deviation (s_{dep}) in MeV of the energy deposition profile of a proton or heavy ion in the SV was adapted from [21]:

$$s_{dep} \approx Z_1 \cdot \sqrt{A} \cdot \sqrt{h_{SV}} \tag{12}$$

where Z_1 is the atomic number of the projectile ion and h_{SV} the SV height in nm. The parameter A in $\mathrm{MeV}^2/\mathrm{nm}$ in above is defined as

$$A = 4\pi(\alpha\hbar c)^2 N Z_2, \tag{13}$$

where $\hbar$ is the reduced Planck's constant. N and Z_2 are the atomic density and the atomic number of the target, respectively. For a silicon target, ($Z_2 = 14$) $A = 1.82 \cdot 10^{-8}\ MeV^2/nm$.

For this work a log-normal shape was assumed for the energy deposition distribution $D(E_{dep})$ within a target of a given thickness, as the domain of the log-normal distribution is strictly positive. For a collection of proton or heavy-ion energy deposition events calculated after the straggling model presented here, the distribution is

$$D(E_{dep}) = \frac{1}{E_{dep} \cdot s_{log} \cdot \sqrt{2\pi}} \cdot \exp\left(-\frac{(ln(E_{dep}) - \mu_{log})^2}{2 \cdot s_{log}^2}\right) \tag{14}$$

The mean (μ_{log}) and the standard deviation (s_{log}) of the log-normal distribution can be calculated from the LET and the straggling models using

$$\mu_{log} = \ln\left(\frac{\langle E_{dep}\rangle^2}{\sqrt{\langle E_{dep}\rangle^2 + s_{dep}^2}}\right) \tag{15}$$

and

$$s_{log}^2 = \ln\left(1 + \frac{s_{dep}^2}{\langle E_{dep}\rangle^2}\right) \tag{16}$$

The average deposited energy $\langle E_{dep}\rangle$ in the SV of height h_{SV} can be calculated from the LET ($\frac{dE}{dx}$) of the particle reaching the SV with an energy of E_{p^+} via

$$\langle E_{dep}\rangle = \frac{dE}{dx}(E_{p^+}) \cdot h_{SV} \tag{17}$$

B. Results

The energy deposition profiles calculated based on the approach described above were compared to Geant4 simulation results. Figures 5 and 6 present probability density distributions of the energy deposition of protons in Si-targets computed via Geant4 [22] simulations and via the straggling model described above. The distributions are normalized so that the area under the distribution equals unity. Figure 5 presents the distributions for various proton energies in a

TABLE I
OVERVIEW OF THE AVERAGE AND STANDARD DEVIATION OF THE RELATIVE DIFFERENCE ($\langle\Delta\rangle \pm s_\Delta$) FOR DIFFERENT MODELS COMPARED TO EXPERIMENTAL DATA. PRESENTED ARE DATA FOR H, HE, O, AR, KR, XE PROJECTILES IN C, AL, NI, SI TARGETS OVER DIFFERENT ENERGY RANGES. THE NUMBER OF DATA POINTS (N_{data}) IN EACH ENERGY RANGE (E_{range}) ARE GIVEN.

E_{range}	Low (<0.1 MeV/u)	Intermediate (0.1-10 MeV/u)	High (>10 MeV/u)	Full
N_{data}	1859	3163	190	5212
This Work	-8.26 ± 28.47	2.08 ± 8.84	11.63 ± 20.80	-1.26 ± 19.56
SRIM	-10.23 ± 37.44	1.70 ± 8.25	8.51 ± 18.48	-2.32 ± 24.28
DPASS	-19.21 ± 39.15	2.94 ± 12.97	6.60 ± 19.60	-4.83 ± 27.89

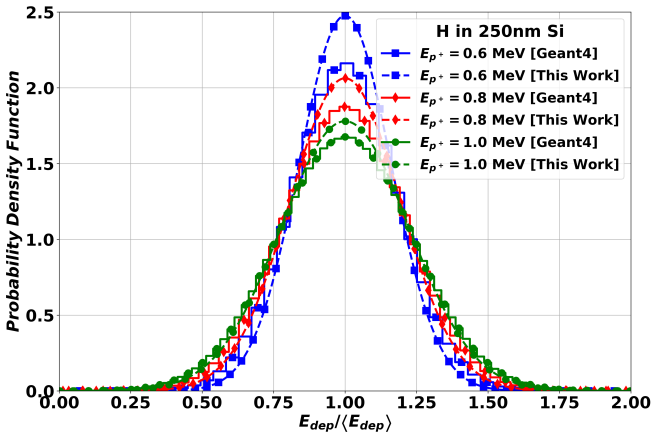

Fig. 5. Probability density functions of the normalized energy depositions of protons in a Si $h_{SV} = 250\,\text{nm}$. Functions for various initial proton energies E_{p^+} are presented. Solid line represent the simulated distribution and the dashed lines the modelled distribution.

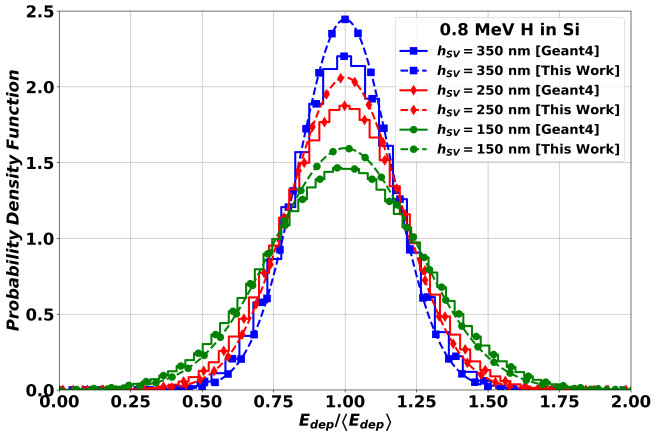

Fig. 6. Probability density functions of the normalized energy depositions of $0.8\,\text{MeV}$ protons in Si. Functions for various h_{SV} are presented. Solid line represent the simulated distribution and the dashed lines the modelled distribution.

Si SV with $h_{SV} = 250$ nm and Fig. 6 the distributions of $0.8\,\text{MeV}$ protons in Si-SVs with varying heights.

Both Fig. 5 and Fig. 6 confirm that the model is able to estimate the width of the distributions compared to Geant4 simulations. Additionally, for the proton energies relevant for this work the probability density function can be represented by a log-normal distribution.

IV. APPLYING THE MODELS TO DETERMINE RPP PARAMETERS

In this section the methodology to estimate the PDI cross-sections for a RPP geometry based on the two models detailed above is presented. This is used further to iteratively determine the RPP parameters for sets of PDI cross-section data.

MC simulations are preformed with RPP geometries from the extracted parameters. The simulated cross-sections are then compared against the experimental cross-section data presented in the literature.

RPP geometries are mainly used in the simulation of radiation environments to estimate the SER of the device under that radiation environment. This has not been done here, as it is beyond of the scope of this work.

A. Method and Calculations

1) Estimation of Proton Energy after Overlayers: The first step in this method is to determine the energy of the primary proton at SV level (E_{SV}) in MeV after traversing the overlayers of thickness h_{OL} in µm of the RPP geometry. Here, the LET model is used to estimate the energy lost by the proton with initial energy E_{p^+} to the overlayers and from that the remaining energy of the particle when reaching the SV level.

The energy at SV level E_{SV} can be estimated from the initial energy of the particle $E_{p^+} = E_0$ by splitting the overlayers in sections of thickness h_{sect}. A section thickness of $200\,\text{nm}$ was used in this work and was chosen as a compromise of computation time and accuracy. The energy after a section E_{post} is calculated by reducing the energy of the particle E_{pre} before entering section by the energy lost in that section. The energy lost is estimated with the LET model and the thickness of the section according to:

$$E_{post} = E_{pre} - \frac{dE}{dx}(E_{pre}) \cdot h_{sect}. \tag{18}$$

This procedure is repeated for every section of the OL until the energy at the SV surface is known. The thickness of the last section has to be adjusted if thickness of the OL is not divisible without rest by the selection section thickness.

The initial guess for the the thickness of the overlayers h_{OL} can be derived from the initial proton energy $E_{p^+,max}$ at which the peak of the experimental PDI cross-section data is observed. It is assumed that the PDI cross-section peak occurs when the Bragg peak of the proton is located in the SV of the RPP geometry. With that assumption an initial estimate for h_{OL} can be made. E.g. for a PDI peak located at $E_{p^+,max} = 0.6\,\text{MeV}$ an initial guess of $7.3\,\mu\text{m}$ of Si-equivalent overlayer would be made, the Bragg peak ranges of protons in several target materials are presented in Fig 7.

In Fig. 7 the Bragg peak ranges calculated via SRIM2013 for Si, SiO_2 and Kapton are shown. The values for Si are also given as estimated using the LET model presented in this work. It shows that both calculations, via the model or SRIM2013, of the location of the Bragg peak agree. Common materials encounter in the packaging and overlayers of devices were chosen for illustration.

Due to the current limitations of the LET model, only elemental overlayers can be considered. For that reason, Si was

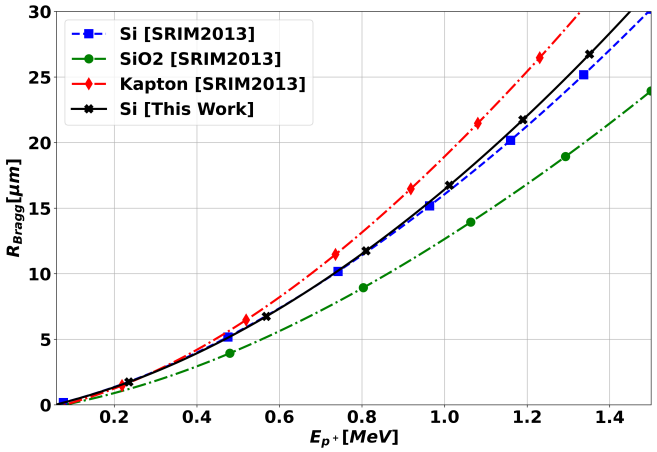

Fig. 7. Proton Bragg peak range (R_{Bragg}) in µm inside Si, SiO_2 and Kapton targets as a function of primary energy (E_{p^+}) in MeV.

chosen as the substitute of SiO_2 for the devices investigated in this work. This will provide an Si equivalent overlayer thickness and all further parameters will be determined with that taken into consideration.

2) Estimation of Deposited Energy Distribution in the SV: With the estimated E_{SV} from the previous step, the previous models are used to determine the parameters μ_{log} and s_{log} for the energy deposition distribution ($D(E_{dep})$) in MeV^{-1} of the proton with energy E_{SV} in the SV of thickness h_{SV}. $D(E_{dep})$ is to be normalized so that:

$$\int_0^\infty D(E_{dep})dE_{dep} = 1 \tag{19}$$

A first guess for h_{SV} and a_{SV} in µm can be made by assuming a cubic SV as follows

$$a_{SV} = h_{SV} = \sqrt{\sigma_{PDI,max}} \tag{20}$$

with $\sigma_{PDI,max}$ being the maximum PDI cross-section of the experimental data in cm^2. This is derived from the assumption that at the Bragg peak energy any proton reaching the SV is able to upset it making the surface area of the SV equal to $\sigma_{PDI,max}$. The SV is assumed cubic as literature shows that a_{SV} and h_{SV} are in the same order of magnitude for the technologies covered here (see Table III), making a cubic SV a reasonable starting point.

3) Application of the Critical Charge Threshold: In this step the critical charge (Q_{crit}) of the RPP geometry is applied to $D(E_{dep})$. First, Q_{crit} in fC is transformed into critical energy (E_{crit}) in MeV according to

$$E_{crit} = Q_{crit} \cdot F \tag{21}$$

where $F = 22.5\mathrm{MeVpC}^{-1}$ describes the energy required to create an electron-hole pair in Si.

E_{crit} is then applied to $D(E_{dep})$ to determine the likelihood $P(E_{p^+}, E_{dep} > E_{crit})$ of a proton with initial energy E_{p^+} inducing an upset by depositing energy (E_{dep}) in the SV above the critical energy (E_{crit}). This is calculated via

$$\begin{aligned} P(E_{p^+}, E_{dep} > E_{crit}) &= \int_{E_{crit}}^\infty D(E_{dep})dE_{dep} \\ &= \frac{1}{2}\mathrm{erfc}\left(\frac{ln(E_{dep}) - \mu_{log}}{s_{log} \cdot \sqrt{2}}\right), \end{aligned} \tag{22}$$

where erfc refers to the complementary error function.

An initial value for Q_{crit} around 0.75 fC can be assumed for this step. No clear correlation between Q_{crit} and the experimental cross-section curve was identified in this work. Therefore, the initial value was derived from Q_{crit} values reported in the literature for similar technology node sizes [4], [5], [9]. The initial value was chosen as the center of the Q_{crit} value range displayed in the literature ($\approx$ 0.5 fC to 1.0 fC).

4) Converting $P(E_{p^+}, E_{dep} > E_{crit})$ into Cross-Section: The estimated cross-section (σ_{est}) of a proton with energy E_{p^+} inducing an upset in the RPP geometry is calculated after

$$\sigma_{est}(E_{p^+}) = P(E_{p^+}, E_{dep} > E_{crit}) \cdot a_{SV}^2, \tag{23}$$

where a_{SV} is the lateral length and of the SV in µm, assuming a square surface of the SV. The initial guess for a_{SV} is made according to Eq. 20.

5) Iterative Adjustment of Parameters: For the last step of the method steps 1) through 4) are performed for the energies used in the experiments and the cross-section estimated based on a initial guess for the RPP geometry. Afterwards, the mean squared error (MSE) between the results of this method and the experimental cross-section is calculated with

$$MSE = \frac{1}{N_{exp}} \sum_{i=1}^{N_{exp}} (\log_{10}(\sigma_{est}(E_i)) - \log_{10}(\sigma_{exp,i}))^2 \tag{24}$$

where N_{exp} is the number of experimental data points, E_i and $\sigma_{exp,i}$ are the i-th pair of proton energy in MeV used in the experiment and measured cross-section in cm^2, respectively.

Then the parameters of the RPP (a_{SV},h_{SV},h_{OL} and Q_{crit}) are adjusted until the MSE is minimized. This can be done either via minimization algorithms or manually. In general, the a_{SV} was observed to impact the vertical offset of the estimated cross-sections, h_{OL} the position of the cross-section peak and h_{SV} in conjunction with Q_{crit} the shape of the right shoulder of the cross-section curve [5].

This method was applied to four SRAM data sets. The sources and technology nodes can be seen in Table II. For all, the RPP parameters were extracted from the experimental data using the method presented here. The resulting RPP geometries were then used in Geant4 MC simulation to compare their ability to reproduce the DUTs PDI SEU behavior in simulations. Finally, the MSE was calculated between the experimental cross-section data and the simulated cross-section data from the literature and from the Geant4 simulations with the RPP geometries determined here, respectively.

TABLE II
DATA SET NAMES, SOURCES AND TECHNOLOGY USED FOR COMPARISON IN THIS WORK

Name	Source	Technology
ISSI	[5], [9]	40 nm[1]
Cypress	[5]	65 nm
RADSAGA	[5]	65 nm
TI	[4]	65 nm

[1] [9] states 65 nm, but [5] correctly states 40 nm.

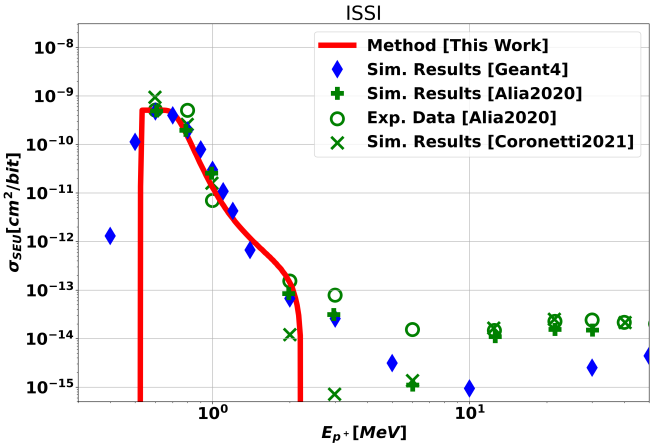

Fig. 8. Proton SEU cross section for the ISSI SRAM. Experimental and simulated data from [9] are presented. Cross-section values calculated from the method presented here based on the determined RPP parameters are shown. Furthermore, results of a MC simulation using Geant4 based on the RPP geometry determined here is displayed.

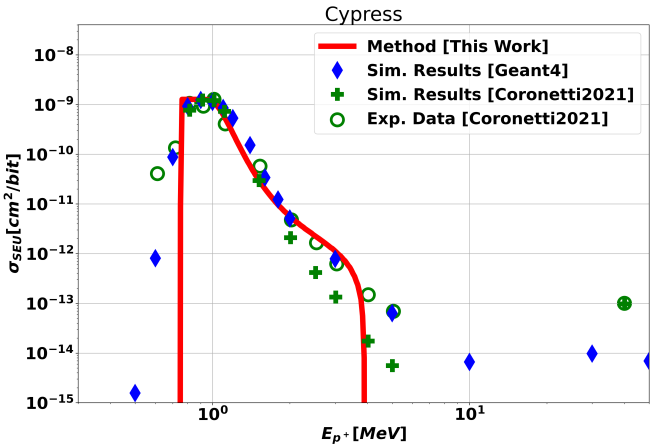

Fig. 9. Proton SEU cross section for the Cypress SRAM. Experimental and simulated data from [5] are presented. Cross-section values calculated from the method presented here based on the determined RPP parameters are shown. Furthermore, results of a MC simulation using Geant4 based on the RPP geometry determined here is displayed.

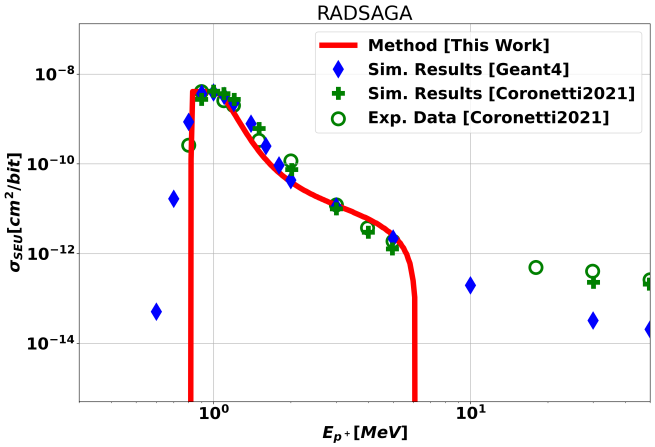

Fig. 10. Proton SEU cross section for the RADSAGA SRAM. Experimental and simulated data from [5] are presented. Cross-section values calculated from the method presented here based on the determined RPP parameters are shown. Furthermore, results of a MC simulation using Geant4 based on the RPP geometry determined here is displayed.

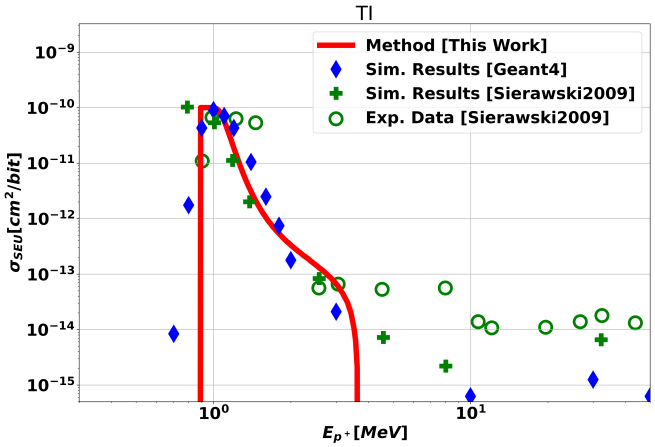

Fig. 11. Proton SEU cross section for the TI SRAM. Experimental and simulated data from [4] are presented. Cross-section values calculated from the method presented here based on the determined RPP parameters are shown. Furthermore, results of a MC simulation using Geant4 based on the RPP geometry determined here is displayed.

B. Results

The RPP parameters for the four data sets determined by this method and the parameters presented in the literature are presented in Table III. Furthermore, the MSE values between the experimental and the Geant4 simulated cross-section data are presented for both the RPP geometries presented in the literature and the ones extracted in this work.

Some of the RPP geometries reported in the literature consist of multiple nested SVs, but only the parameters of the central SV were used for the comparison. This has been done since a single SV is sufficient to emulate the LEP SEU response, which is the focus of this work. The nested SVs were introduced in the literature to better emulate the high energy proton SEU response, as well as the heavy ion SEU response.

Figures 8 through 11 show the experimental and simulated cross-section data from the literature for the four data sets, as well as the cross-sections based on the RPP geometry determined in this work estimated using the method described here and Geant4 MC simulation results of the same RPP geometry.

The proposed method is able to reproduce the RPP parameters that are close to the ones reported in the literature strictly numerically without the use of the MC method. Furthermore, the obtained parameters were confirmed to reproduce the PDI cross-sections of the DUTs in MC simulations with comparable accuracy as the simulations performed in the literature.

Additionally, the MC simulations and the method return comparable cross-section values when performed for a given RPP geometry, apart from the left side of the cross-section peak, because the method does not take straggling inside the overlayers into account. This confirms the method's use as a replacement of the MC simulation during the iterative adjustment of the RPP parameters.

Finally, it has been shown that assuming an elemental Si overlayer with a Si equivalent overlayer thickness did not induce any significant uncertainty in the MC simulation results, which were able to accurately reproduce the experimental PDI data with a purely elemental overlayer.

TABLE III
RPP PARAMETERS FOR THE 4 DATA SETS DISCUSSED IN THIS WORK. VALUES FROM THE LITERATURE (IF AVAILABLE) AND VALUES DETERMINED BY THE METHOD PRESENTED IN THIS WORK ARE GIVEN. THE MSE BETWEEN THE MC SIMULATED AND THE EXPERIMENTAL DATA IS PRESENTED.

Device	Source	a_{SV} $[\mu m]$	h_{SV} $[\mu m]$	h_{OL} $[\mu m]$	Q_{crit} $[fC]$	MSE $[\log_{10}(\mathrm{cm}^2)^2]$
ISSI	[9]	0.25	0.25	6.0	0.73	0.147
	[5]	0.31	0.31	6.0	0.96	1.012
	This Work	0.225	0.25	6.5	0.73	0.186
Cypress	[5]	0.36	0.36	10.0	0.86	0.384
	This Work	0.356	0.356	11.0	0.8	0.071
RADSAGA	[5]	0.638	0.25	12.0	0.55	0.139
	This Work	0.638	0.28	12.5	0.63	0.066
TI	[4]	-	-	-	-	0.593
	This Work	0.1	0.25	14	0.65	0.221

V. DISCUSSION AND FURTHER WORK

A. LET Model

The LET model itself agrees well in comparison with well established LET softwares, SRIM2013 [29] and DPASS [30], for protons and heavy ions in various elemental targets. In contrast to the establish softwares, the proposed model is available as a collection of equations. This makes this model very versatile and able to support the presented method without the need of external software. Furthermore, it is natively supports any platform able to perform numerical calculations and can therefore be easily implemented in programming algorithms such as the method described here.

The model is not limited to protons and covers a projectile range from H to Au and targets from Li until Au. As of now, only elemental solid targets can be considered. No direct functional relation was found between parameters p_0 and p_1 and the characteristics of the projectile-target combination. Therefore, the current version of the model interpolates parameters p_0 and p_1 over Z_1 and Z_2 for projectile-target combinations, that could not used in the fitting process due to insufficient or no data in the NDS database [23]. This may result in inaccurate parameters, when projectile-target combinations are considered that have no fitted data set close to them. Since, H in Si was one of the data sets used in the fitting procedure, this limitation does not apply to the method described here.

The next steps in developing this model are to find a functional relationship between the projectile-target combinations and p_0 and p_1, and to expand the model to cover non-elemental targets as well, most importantly compounds used in electronics, such as SiO_2 and SiC.

B. Straggling Model

The straggling model has been shown to provide accurate estimates on the energy deposition distributions for protons in the energy and target thickness ranges relevant to low energy proton testing of devices in modern technologies. The models straightforward equations make it simple to implement in low computing power calculations.

The accuracy of the model declines when the range of the particle is close to or lower than the thickness of the absorber. This impacts mostly energies left of the PDI cross-section peak. Due to the high average deposited energy around the Bragg peak and low h_{SV} associated with the newer technologies in the literature this has little impact on the method.

Further research into the straggling model is planned to improve the characterization of the straggling close to or at end of range of the particle.

C. Applying the Models to Determine RPP parameters

The method presented in this work was shown to successfully estimate PDI cross-section values based on a RPP geometry and then was used to iteratively determine RPP parameters for LEP cross-section data sets. Furthermore, the method proofed to accurately predict MC simulations PDI cross-section results results for a given RPP geometry.

The methods ability to emulate the results of MC simulations was successfully benchmarked by performing Geant4 MC simulations with the four RPP geometries determined here, without using the MC method at any step in the determination of those parameters. The results of the simulations agree well with the values estimated by the method based on the same RPP geometry. The results of the Geant4 simulations of the RPP geometries also agree with the experimental and the simulated cross-section values from the literature, validating the method's use in the determination of RPP geometries from experimental PDI cross-section data.

Due to the non-reliance of this method on the MC method of external software, the determination of the RPP parameters for each data set can be performed within minutes. The reduced time and computation power requirements makes this method an attractive alternative to repeated MC simulations to determine a single SV RPP geometry based on PDI cross-section data. The determination of the RPP parameters took approximately $10\,\mathrm{min}$ per data set, whereas the MC simulation of one set of RPP parameters took $4\,\mathrm{h}$ each.

Currently, the presented method only takes the straggling inside the SV into account. This causes the estimated cross section peak to exhibit a very steep decrease with decreasing proton energy below the PDI SEU cross section maximum, because it consider all particles with an average range below h_{OL} not to reach the SV. Due to straggling, even if the average range of the particles is too low, a fraction of the particles will still penetrate the overlayers, potentially upsetting the device. This has to be taken into account when interpreting the results.

Furthermore, the LET model covers only elemental targets, which means the materials used in the algorithm are limited to elemental materials as well. This will only affect h_{OL} as this most commonly assumed as SiO_2 or Si depending on the device. As of now, this method only can only consider Si and therefore gives slightly increased values for h_{OL} compared to the literature values, when SiO_2 was used there.

It has little to no influence in the accuracy of the MC simulations, in which Si was used as well, in comparison to the experimental values. Essentially, the SiO_2 overlayer thickness is translated into a Si equivalent thickness. An elemental material close to the assumed, or known, overlayer material composition should be chosen. This may be a cause of error for very complex overlayer compositions or for materials where it is more difficult to choose a suitable elemental material such as polymers and similar complex materials. Further investigations may be required to find elemental materials with similar stopping characteristics as the assumed, or known, overlayer materials. Even in those cases, the uncertainties are expected to be minimal as the method uses the same elemental material to determine the remaining parameters providing a RPP geometry that will reproduce the experiment values in MC simulation based on the chosen overlayer material.

Additionally, due to the underlying models' limitations to direct ionization effects, the method can not provide cross-sections at higher energies, where nuclear reactions dominate the ionization. Therefore, when the PDI peak of the DUT's SEU response overlaps with the indirect ionization response, the model will not be able to reproduce these values accurately. Therefore, the method will be subject to increased uncertainties for $h_{OL} \gg 10\,\mu\mathrm{m}$.

The simulated cross-section data based on the determined RPP parameters in this work show differences for the high energy proton (HEP) cross-section data, while showing good agreement with the low energy proton cross-section data. This is not unexpected since it has been shown that high energy proton and heavy ion cross-section data require multiple nested SVs to be accurately represented in MC simulations [5], [9]. The nested volumes around the central SV use the same Q_{crit} but a reduced charge collection efficiency is assumed, meaning only a fraction of the charge produced within the nested SV by the incoming particle is collected by the volume. LEPs are not able to produce an upset when depositing energy in the outer nested SVs due to the reduced charge collection efficiency. Only heavy ions and secondaries from nuclear reactions, induced by high energy protons, are able to deposit sufficient energy in the nested SV due to their higher LET compared to LEPs. Therefore, only the center SV, having 100% charge collection efficiency by definition, can be derived from the PDI cross-section data. This method, currently, focuses only on direct ionization effects from protons and therefore can only extract information for a single SV RPP geometry from LEP PDI cross section data. In order to extend the RPP geometry with nested volumes either heavy ion or HEP cross-section data has to be available and be taken into consideration. The more data points are available the more detailed the description of the nested RPP geometry will be. This is not the focus of this work and the extraction of RPP parameters from heavy ion data has been presented in [17], [18]. The goal of this work is the numerical extraction of RPP parameters from PDI cross-section for error rate calculations and MC simulations.

The metric of MSE was applied in this work to quantitatively assess the agreement of the cross-section values estimated by the method and the experimental data. It enables the method to determine the set of RPP parameters that most accurately emulate the device's SEU response in MC simulation. Cross-sections estimated by the method agree with cross-section obtained from MC simulations for the same RPP geometries. This set of parameters will exhibit the lowest MSE between the method's results and the experimental data.

This method will be extended to include the straggle occurring in the overlayers, extending the applicability of it to higher overlayer thicknesses, and with that data obtained during backside irradiations where the beam needs to penetrate tens of micrometers of thinned substrate before reaching the SV. Furthermore, it is planned to direct ionization effects of heavy ions. Additionally, the applicability of this method for smaller technologies will be investigated. Once the LET model is able to cover compound targets, this method will also cover those materials in the overlayers.

Finally, it is important to note, that this method does not aim to replace the MC method for the calculation of cross-sections from RPP geometries, as the MC method is more flexible and accurate. The main objective of this method is to replace excess MC simulations during the initial adjustment of RPP parameters. The extracted RPP geometry can then be used as a surrogate for the DUT in MC simulations of radiation environments to estimate the LEP SEU response of the DUT under that environment. Overall, this greatly reduces the amount of MC simulations necessary in this process.

VI. Conclusions

RPP geometries are typically used in MC simulations to estimate the SER of a DUT under a given radiation environment. The process of finding the set of RPP parameters that emulates the DUT's PDI SEU response can be time consuming and difficult as various sets of parameters might need to be simulated until one has found a set that recreates the DUT's response satisfyingly. Therefore, aim of this work was to provide a method to determine RPP parameters from PDI cross-section data quicker and easier. This method is based on two numerical models, that describe (1) the linear energy transfer, from which the average energy deposition can be derived, and (2) the standard deviation of the energy deposition distributions for protons and other ions traversing elemental solid targets. Both of these models were described and benchmarked against experimental stopping power values from the NDS and MC simulated energy deposition profiles. Both models exhibit adequate accuracy for their simplicity. The two models when combined enables estimation of cross-sections based on RPP geometries. This in turn can be utilized to iteratively determine RPP parameters for devices for which experimental low energy proton SEU cross-section data are available. The RPP parameters determined with this procedure were used in MC simulations and the obtained results agree with the experimental and simulation results presented in the literature.

Despite the method's limitations and simplicity compared to the MC method, it is demonstrated that the RPP parameters determined by the using the proposed method are in good agreement with those obtained from more traditional MC approach. The method offers great reduction in demand of computing power and time, which makes this method a viable approach to determine RPP parameters from experimental LEP SEU data. But due to its inherent limitations in terms of energies that can be used and effects considered, it

is not intended replace the MC method beyond the use cases presented here.

Finally, it is to note that the use of the new LET model presented here is not limited only to protons in silicon, but it on its own provides a tool to estimate heavy ion stopping in any elemental solid target.

REFERENCES

[1] N. A. Dodds *et al.*, "Hardness assurance for proton direct ionization-induced SEEs using a high-energy proton beam," *IEEE Transactions on Nuclear Science*, vol. 61, no. 6, pp. 2904–2914, 2014.

[2] N. A. Dodds *et al.*, "The Contribution of Low-Energy Protons to the Total On-Orbit SEU Rate," *IEEE Transactions on Nuclear Science*, vol. 62, no. 6, pp. 2440–2451, 2015.

[3] J. A. Pellish *et al.*, "Criticality of Low-Energy Protons in Single-Event Effects Testing of Highly-Scaled Technologies," *IEEE Transactions on Nuclear Science*, vol. 61, no. 1, pp. 2896–2903, 2014.

[4] B. D. Sierawski *et al.*, "Impact of low-energy proton induced upsets on test methods and rate predictions," *IEEE Transactions on Nuclear Science*, vol. 56, no. 6, pp. 3085–3092, 2009.

[5] A. Coronetti *et al.*, "Assessment of Proton Direct Ionization for the Radiation Hardness Assurance of Deep Submicron SRAMs Used in Space Applications," *IEEE Transactions on Nuclear Science*, vol. 68, no. 5, pp. 937–948, 2021.

[6] K. P. Rodbell *et al.*, "Low-Energy Proton-Induced Single-Event-Upsets in 65 nm Node, Silicon-on-Insulator, Latches and Memory Cells," *IEEE Transactions on Nuclear Science*, vol. 54, no. 6, pp. 2474–2479, 2007.

[7] K. P. Rodbell, "Low-Energy Protons - Where and Why 'Rare Events' Matter," *IEEE Transactions on Nuclear Science*, vol. 67, no. 7, pp. 1204–1215, 2020.

[8] E. H. Cannon *et al.*, "Heavy Ion, High-Energy, and Low-Energy Proton SEE Sensitivity of 90-nm RHBD SRAMs," *IEEE Transactions on Nuclear Science*, vol. 57, no. 6, pp. 3493–3499, 2010.

[9] R. Garcia Alia *et al.*, "Direct ionization impact on accelerator mixed-field soft-error rate," *IEEE Transactions on Nuclear Science*, vol. 67, no. 1, pp. 345–352, 2020.

[10] N. Seifert *et al.*, "The Susceptibility of 45 and 32 nm Bulk CMOS Latches to Low-Energy Protons," *IEEE Transactions on Nuclear Science*, vol. 58, no. 6, pp. 2711–2718, 2011.

[11] K. P. Rodbell, M. S. Gordon, K. G. Stawiasz, P. Oldiges, K. Lilja, and M. Turowski, "Low Energy Proton SEUs in 32-nm SOI SRAMs at Low Vdd," *IEEE Transactions on Nuclear Science*, vol. 64, no. 3, pp. 999–1005, 2017.

[12] J. Guillermin, N. Sukhaseum, P. Pourrouquet, N. Chatry, F. Bezerra, and R. Ecoffet, "Worst-Case Proton Contribution to the Direct Ionization SEU Rate," *2017 17th European Conference on Radiation and Its Effects on Components and Systems, RADECS 2017*, pp. 330–337, 2017.

[13] J. A. Pellish *et al.*, "Impact of Spacecraft Shielding on Direct Ionization Soft Error Rates for sub-130 nm Technologies," *IEEE Transactions on Nuclear Science*, vol. 57, no. 6, pp. 3183–3189, 2010.

[14] G. Hubert, S. Duzellier, F. Bezerra, and R. Ecoffet, "MUSCA SEP3 contributions to investigate the direct ionization proton upset in 65nm technology for space, atmospheric and ground applications," *Proceedings of the European Conference on Radiation and its Effects on Components and Systems, RADECS*, pp. 179–186, 2009.

[15] R. A. Weller *et al.*, "General Framework for Single Event Effects Rate Prediction in Microelectronics," *IEEE Transactions on Nuclear Science*, vol. 56, no. 6, pp. 3098–3108, 2009.

[16] R. A. Weller *et al.*, "Monte Carlo simulation of single event effects," *IEEE Transactions on Nuclear Science*, vol. 57, no. 4 PART 1, pp. 1726–1746, 2010.

[17] R. García *et al.*, "Calibration of the weighed sensitive volume model to heavy ion experimental data," *Proceedings of the European Conference on Radiation and its Effects on Components and Systems, RADECS*, vol. M, pp. 60–66, 2011.

[18] R. García *et al.*, "Combined use of heavy ion and proton test data in the determination of a GaAs power MESFET critical charge and sensitive depth," *Proceedings of the European Conference on Radiation and its Effects on Components and Systems, RADECS*, pp. 244–251, 2011.

[19] J. M. Trippe *et al.*, "Predicting Muon-Induced SEU Rates for a 28-nm SRAM Using Protons and Heavy Ions to Calibrate the Sensitive Volume Model," *IEEE Transactions on Nuclear Science*, vol. 65, no. 2, pp. 712–718, 2018.

[20] L. de Ferrariis and N. R. Arista, "Classical and quantum-mechanical treatments of the energy loss of charged particles in dilute plasmas," *Phys. Rev. A*, vol. 29, pp. 2145–2159, Apr 1984.

[21] A. Javanainen *et al.*, "Semi-empirical model for SEGR prediction," *IEEE Transactions on Nuclear Science*, vol. 60, no. 4, pp. 2660–2665, 2013.

[22] S. Agostinelli *et al.*, "GEANT4 - A simulation toolkit," *Nuclear Instruments and Methods in Physics Research, Section A: Accelerators, Spectrometers, Detectors and Associated Equipment*, vol. 506, no. 3, pp. 250–303, 2003.

[23] H. Paul, "NDS database for electronic stopping power of matter for ions." https://www-nds.iaea.org/stopping/index.html. Accessed: 03.10.2019.

[24] P. Sigmund, "Stopping of Heavy Ions," *Springer Tracts in Modern Physics*, 2004.

[25] N. Bohr, "LX. On the decrease of velocity of swiftly moving electrified particles in passing through matter," *The London, Edinburgh, and Dublin Philosophical Magazine and Journal of Science*, vol. 30, no. 178, pp. 581–612, 1915.

[26] J. Lindhard and M. Scharff, "Energy Dissipation by Ions in the kev Region," *Physical Review*, vol. 124, no. 1, pp. 128–130, 1961.

[27] B. Firsov, "A qualitive interpretation of the mean electron excitation energy in atomic collisions," *J. Exptl. Theoret. Phys. (U.S.S.R.)*, vol. 36, no. 9, pp. 1517–1523, 1959.

[28] S. Lüdeke and A. Javanainen, "Semi-empirical parameters for electronic stopping force model. Relative differences between experimental data and various stopping models (this model, SRIM2013, DPASS)." https://jyx.jyu.fi/handle/123456789/78898. DOI: 10.17011/jyx/dataset/78898.

[29] J. F. Ziegler, "SRIM-2003," *Nuclear Instruments and Methods in Physics Research, Section B: Beam Interactions with Materials and Atoms*, vol. 219-220, pp. 1027–1036, 2004.

[30] A. Schinner and P. Sigmund, "Dpass2.11." https://www.sdu.dk/en/DPASS. Accessed: 03.10.2019.

[31] H. Paul and D. Sánchez-parcerisa, "A critical overview of recent stopping power programs for positive ions in solid elements," *Nuclear Inst. and Methods in Physics Research, B*, vol. 312, pp. 110–117, 2013.